Journal of Materials Science: Materials in Electronics (2018) 29:12323–12329
https://doi.org/10.1007/s10854-018-9345-0

Structure and electrical properties of $(0.99-x)K_{0.5}Na_{0.5}Nb_{0.96}Sb_{0.04}O_3$-$0.01BaZrO_3$-$xBi_{0.5}Na_{0.5}ZrO_3$ lead-free piezoelectric ceramics

Jian Ma[2] · Bo Wu[1] · Wenjuan Wu[1] · Min Chen[1]

Received: 12 April 2018 / Accepted: 23 May 2018 / Published online: 25 May 2018

Abstract
Lead-free $(0.99-x)K_{0.5}Na_{0.5}Nb_{0.96}Sb_{0.04}O_3$-$0.01BaZrO_3$-$xBi_{0.5}Na_{0.5}ZrO_3$ (KNNS–BZ–BNZ) piezoelectric ceramics were fabricated by the conventional solid-state reaction method. The effects of the addition of $Bi_{0.5}Na_{0.5}ZrO_3$ on phase structure, microstructure, and electrical properties were studied in detail. The rhombohedral–tetragonal (R–T) phase boundary was established in the ceramics with $0.03 \le x \le 0.04$. Owing to the both R–T phase boundary and the enhancement of dielectric and ferroelectric properties, an optimal electrical property (e.g., $d_{33} = 450 \pm 5$ pC/N, $k_p = 0.50 \pm 0.02$, and $T_C = 252$ °C) was attained in the ceramics with $x = 0.03$. As a result, constructing phase boundary is proved to be a good way to improve the electrical properties in KNN-based ceramics.

1 Introduction

Piezoelectric materials are widely used in kinds of electron devices, such as sensors, actuators and so on, because of their unique properties which can convert mechanical energy into electrical energy and vice versa [1, 2]. Lead zirconate titanate (PZT) family is governing the piezoelectric market due to their superior piezoelectric properties [3]. However, in order to achieve the sustainable development, it is imperative to develop high-performance Pb-free piezoceramics to replace the Pb-based ones because of the high toxicity of Pb element [4–35].

Potassium-sodium niobate (KNN) ceramics, which are the most promising among the Pb-free piezoceramics, have received considerable attentions due to their good peizoelectric properties and high Curie temperature (T_C) [5–7, 29]. In the past decades, numerous efforts have been carried out to enhance the electrical properties of KNN-based ceramics with the purpose of replacing the Pb-based piezoceramics [5–7, 29]. Some approaches are currently employed to improve the electrical properties in KNN-based ceramics, such as constructing phase boundary [5, 9], new sintering methods [8], new preparation method [10]. Constructing phase boundary is the most promising one among these approaches [5, 9, 12–15, 29, 34]. In particular, a large d_{33} of 416 pC/N as well as a high T_C of 250 °C was obtained in a well-designed textured ceramics [$(K_{0.44}Na_{0.52}Li_{0.04})(Nb_{0.86}Ta_{0.10}Sb_{0.04})O_3$, (LF4T)] possessing an orthorhombic–tetragonal (O–T) phase boundary by Saito et al. who adopted the reactive templated grain growth (RTGG) method [10]. Very recently, Wu's group observed two large d_{33} values of 490 pC/N and 570 pC/N in $(1-x)(K_{1-y}Na_y)(Nb_{1-z}Sb_z)O_3$-$xBi_{0.5}(Na_{1-w}K_w)_{0.5}ZrO_3$ ceramics and $(1-x-y)(K_{1-w}Na_wNb_{1-z}Sb_zO_3$-$yBaZrO_3$-$Bi_{0.5}K_{0.5}HfO_3)$ ceramics, respectively [14, 15]. They attributed the superior piezoelectric properties to the appearance of R–T phase boundary. In spite of the high cost of RTGG method and the relatively low T_C values (< 250 °C) at the optimal piezoelectric properties in Wu's ceramics, constructing phase boundary shows a crucial role in the improvement of electrical properties in KNN ceramics. According to previous works, Sb^{5+}, $BaZrO_3$, and $Bi_{0.5}Na_{0.5}ZrO_3$ can effectively affect the phase structure and electrical properties of KNN ceramics [16–19, 29]. Therefore, these additives are good candidates for constructing phase boundary.

In this work, with the purpose of constructing phase boundary and obtaining high piezoelectric properties, we designed a new formula, $(0.99-x)K_{0.5}Na_{0.5}Nb_{0.96}Sb_{0.04}O_3$-$0.01BaZrO_3$-$xBi_{0.5}Na_{0.5}ZrO_3$ (KNNS–BZ–BNZ) and then

✉ Bo Wu
wubo7788@126.com

[1] Sichuan Province Key Laboratory of Information Materials and Devices Application, Chengdu University of Information Technology, Chengdu 610225, People's Republic of China

[2] Physics Department, Sichuan Province Key Laboratory of Information Materials, Southwest Minzu University, Chengdu 610041, People's Republic of China

prepared the KNNS–BZ–BNZ ceramics by using the conventional solid-state reaction method. Effects of the addition of $Bi_{0.5}Na_{0.5}ZrO_3$ on the phase structure and electrical properties were systematically studied. Both XRD patterns and the temperature dependence of dielectric constant curves attested the formation of R–T phase boundary in the ceramics with $0.03 \le x \le 0.04$, and their electrical properties were improved. The related physical mechanisms were addressed.

2 Experimental procedure

Lead-free KNNS–BZ–BNZ ($0.03 \le x \le 0.04$) piezoelectric ceramics were synthesized by the conventional solid-state reaction method. The raw materials were K_2CO_3 (99%), Na_2CO_3 (99.8%), Nb_2O_5 (99.5%), Sb_2O_3 (99.99%), $BaCO_3$ (99%), Bi_2O_3 (99.999%), and ZrO_2 (99%). All these raw materials were accurately weighed according to the formula by using a high precise electronic balance, and then were ball milled for 20 h with the ethyl alcohol. After drying, the powders were calcined at 850 °C for 6 h, and then were mixed with a binder of 8 wt% polyvinyl alcohol (PVA) and pressed into pellets with a diameter of 10 mm and a thickness of 1 mm. After evaporating PVA, the green disks were sintered at 1080–1125 °C for 3 h. In order to measure the electrical properties, the as-sintered samples were printed with silver paste on the both sides, and then heated at 650 °C for 20 min to form the electrode. Finally, the samples were poled at room temperature for 30 min in a silicon oil bath, by applying a direct current (*dc*) electric field of 3 kV/mm.

The crystal structure was collected by the X-ray diffraction patterns (Bruker D8 Advanced XRD, Bruker AXS Inc., Madison, WI, CuKα). The surface morphology of the as-sintered samples and their elements distribution were measured by a filed-emission scanning electron microscope (FE-SEM, JSM-7500, Japan) accompanied by Energy Dispersive X-ray (EDX) spectroscopy. The dielectric constant (ε_r) varying with temperature (− 150 to 200 °C and 25–400 °C) was measured by using an LCR analyzer (HP 4980, Agilent, USA) in connection with a temperature-controlled instrument. The ferroelectric loops of the ceramics were measured by using a ferroelectric tester (Radiant Technologies, Inc., Albuquerque, NM) at 10 Hz. The planar electromechanical coupling coefficient (k_p) was measured by a resonance-antiresonance method with an impedance analyzer (Impedance Analyzer, PV70A, Beijing). The piezoelectric constant (d_{33}) of the poled samples was measured by using a quasi-static d_{33} meter (ZJ-3A, China). In order to measure the thermal stability, the poled samples were heated for 30 min at the scheduled temperatures and then their d_{33} values were measured.

3 Results and discussion

Figure 1a shows the XRD patterns of the KNNS–BZ–BNZ ceramics as a function of x. All samples display a pure perovskite structure without the occurrence of secondary phases, indicating that $Bi_{0.5}Na_{0.5}ZrO_3$ can effectively diffused into KNN ceramics. Figure 1b shows the enlarged XRD patterns of the samples in the 2 theta range of 44°–47°. The phase structure of the samples is strongly dependent on the content of $Bi_{0.5}Na_{0.5}ZrO_3$. For the ceramics with $x = 0$ and 0.01, a typical orthorhombic (O) phase structure with I_{202}/I_{020} near to 2:1 [I_{202} and I_{020} represent the intensity of diffraction peak (202) and (020), respectively] was observed [20]. As the content of $Bi_{0.5}Na_{0.5}ZrO_3$ increased, I_{202} decreased and I_{020} increased. A ratio of 1:1 and 1:2 between

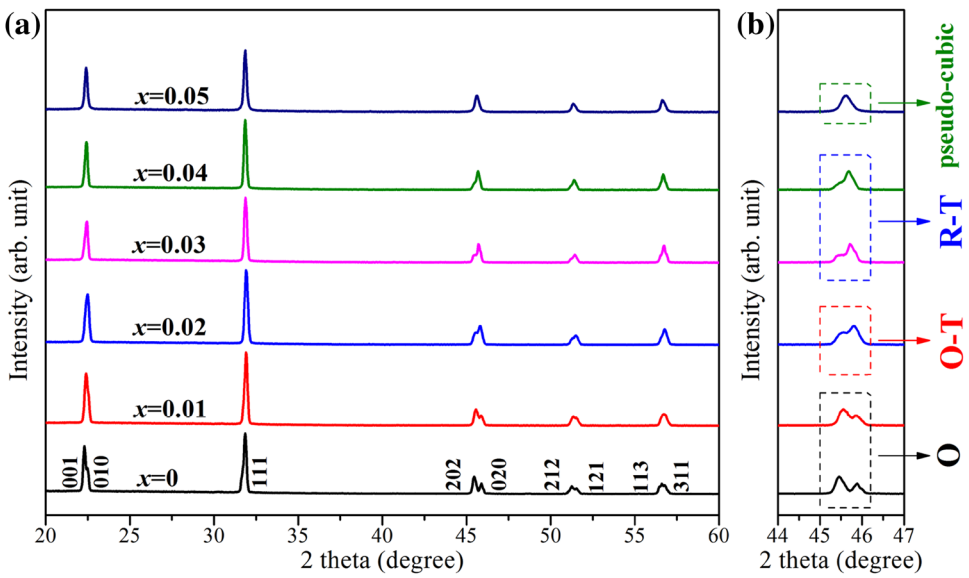

Fig. 1 XRD patterns of the KNNS–BZ–BNZ ceramics in the two theta range of **a** 20°–60°, and **b** 44°–47°

I_{202} and I_{020} were observed in the ceramics with $x=0.02$ and 0.03, respectively, indicating that a tetragonal (T) phase structure was involved [21]. As the content of $Bi_{0.5}Na_{0.5}ZrO_3$ was further increased, a single diffraction peak was observed in the ceramics with $x=0.05$, which was regarded as rhombohedral (R) or pseudo-cubic phase [20, 21].

In order to further analyze the phase structure of KNNS–BZ–BNZ ceramics, the temperature (− 150 to 200 °C) dependence of dielectric constant (ε_r–T) curves were measured, as shown in Fig. 2a–f. From Fig. 2a, two abnormal dielectric peaks were observed, which corresponded to the R–O phase transition ($T_{R-O}=-75$ °C) and O–T phase transition ($T_{O-T}=127$ °C), respectively. With an increase of x, T_{R-O} increased and T_{O-T} dropped. Then, only one abnormal dielectric peak was observed in the ceramics with $x=0.03$ (see Fig. 2d), indicating that both T_{R-O} and T_{O-T} were shifted to the same temperature leading to the formation of R–T phase boundary. As x further increased, T_{R-T} vanished and only one abnormal dielectric peak corresponding to Curie temperature (T_C) was observed in the ceramics with $x=0.05$ (see Fig. 2f), which can be explained by the small grains (see Fig. 4d), and the similar phenomenon was observed in other lead-free ceramics [31–33]. Therefore, combined with XRD patterns and ε_r–T curves, a conclusion on phase structure can be obtained, that is, the ceramics with $x=0$ and 0.01 have an O phase, the ceramics with $x=0.02$ possess an O–T coexistence phase, the ceramics with $x=0.03$ and 0.04 own a R–T coexistence phase and the ceramics with $x=0.05$ are pseudo-cubic phase.

Figure 3a depicts the ε_r–T curves measured at the temperature range of 25–400 °C. It is found that T_C gradually dropped as the content of $Bi_{0.5}Na_{0.5}ZrO_3$ increased. In addition, a relatively high T_C value of 252 °C was obtained in the ceramics with $x=0.03$ which possessed the optimal piezoelectric properties, as discussed later. After deriving T_{R-O}, T_{O-T}, T_{R-T}, and T_C from Figs. 2 and 3a, the phase diagram of the KNNS–BZ–BNZ ceramics was established, as shown in Fig. 3b. According to previous references [19], the addition of $Bi_{0.5}Na_{0.5}ZrO_3$ can elevate T_{R-O} and drop T_{O-T} and T_C, which is also attested in this work. As the content of $Bi_{0.5}Na_{0.5}ZrO_3$ increased, both T_{O-T} and T_C decreased and T_{R-O} increased. Increasing T_{R-O} and decreasing T_{O-T} compressed and even vanished the zone of O phase, leading to the formation of R–T phase boundary.

Figure 4 shows the SEM surface morphology of the KNNS–BZ–BNZ ceramics as a function of x. For the ceramic with $x=0$, an inhomogeneous grain size distribution, which was that the large grains were surrounded by the small ones, was observed. As the x increased from 0 to 0.03, the grain size gradually increased, suggesting that an appropriate content of $Bi_{0.5}Na_{0.5}ZrO_3$ can promote the grain growth [22]. As the x was further increased from 0.03

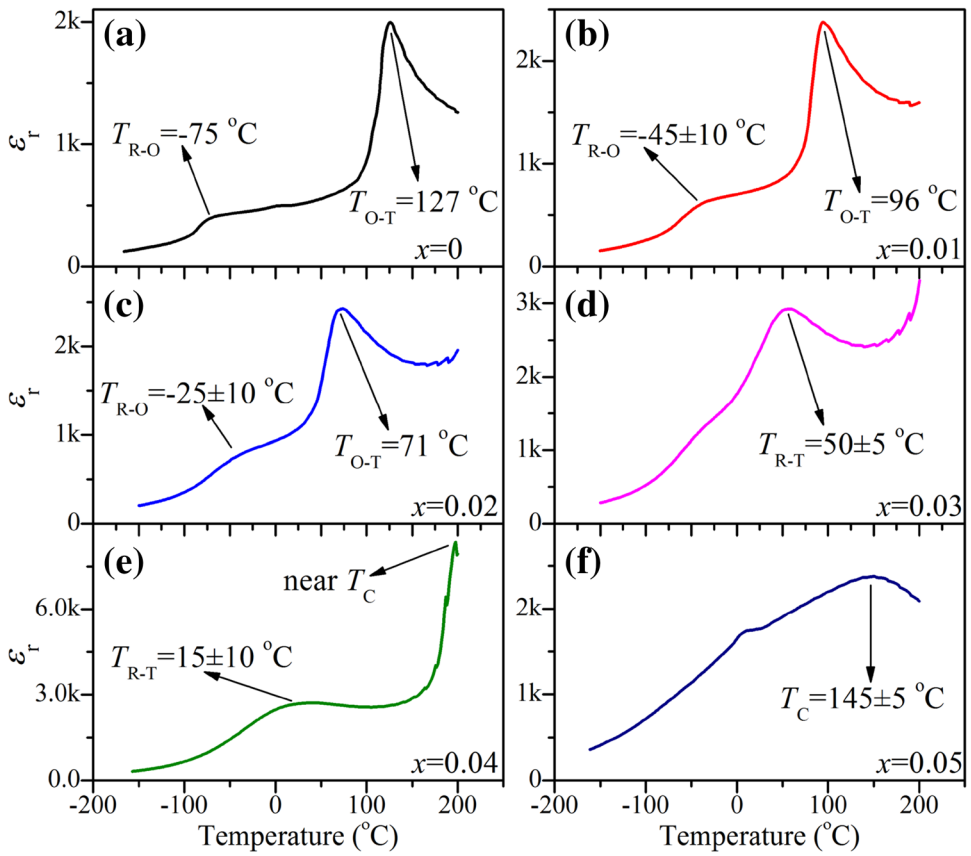

Fig. 2 Temperature (− 150 to 200 °C) dependence of dielectric constant curves of the KNNS–BZ–BNZ ceramics with **a** $x=0$, **b** $x=0.01$, **c** $x=0.02$, **d** $x=0.03$, **e** $x=0.04$, and **f** $x=0.05$

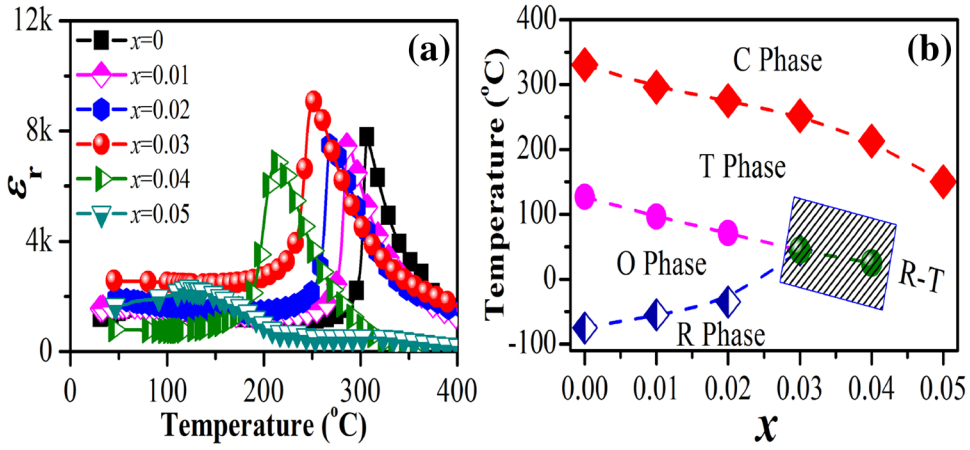

Fig. 3 **a** Temperature (25–400 °C) dependence of dielectric constant curves and **b** phase diagram of the KNNS–BZ–BNZ ceramics as a function of x

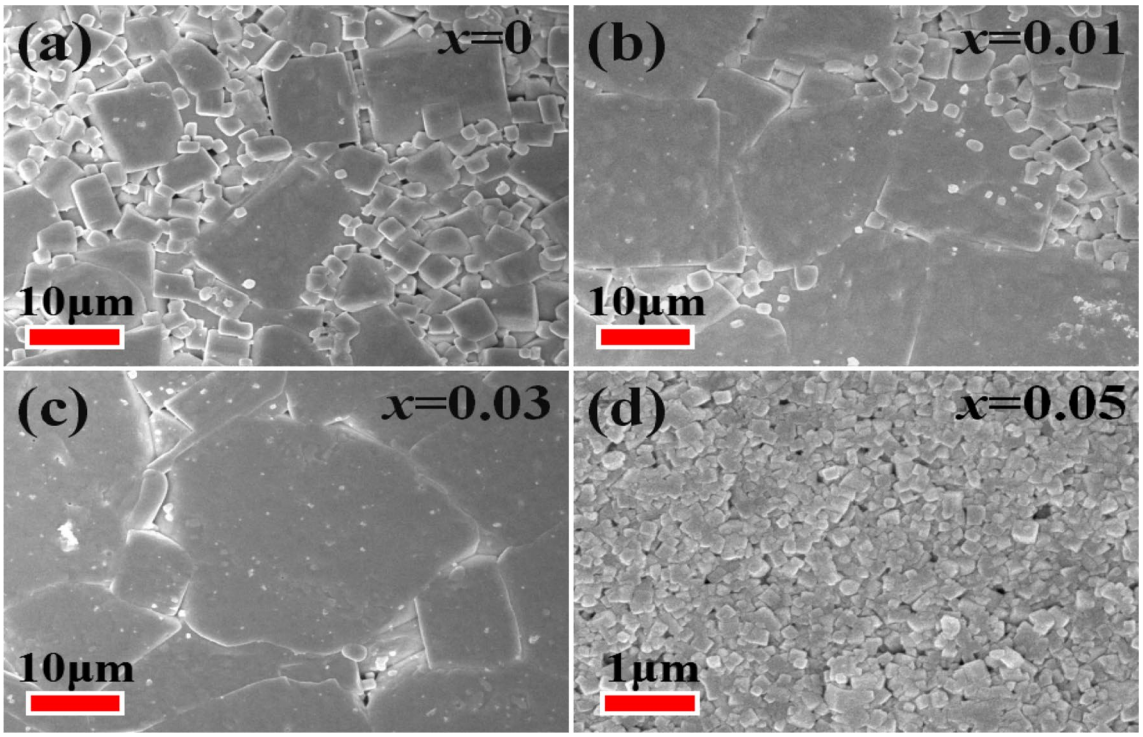

Fig. 4 Surface morphology images of the KNNS–BZ–BNZ ceramics with **a** $x=0$, **b** $x=0.01$, **c** $x=0.03$, and **d** $x=0.05$

to 0.05, the grain size sharply dropped, indicating that high doping content of $Bi_{0.5}Na_{0.5}ZrO_3$ greatly inhibits the grain growth. When the content of $Bi_{0.5}Na_{0.5}ZrO_3$ is high, a small amount of $Bi_{0.5}Na_{0.5}ZrO_3$ aggregates at the grain boundary and then inhibits the grain growth [22]. Considering that eight elements (i.e., K, Na, Nb, Sb, O, Zr, Bi, Ba) are involved in this work, therefore it is necessary to figure out the distribution of these elements. Figure 5 shows the elements mappings of the ceramics with $x=0.03$. It is found that a homogeneous distribution is observed for all elements, indicating a good chemical homogeneity.

Figure 6a shows the ferroelectric loops of the KNNS–BZ–BNZ ceramics as a function of x. All ceramics, except for $x=0.05$, display a classical ferroelectric loops. The deteriorative ferroelectric loop of the ceramics with $x=0.05$ mainly attributed to the pseudo-cubic phase. As we know, a material with high symmetry possesses a poor ferroelectricity and vice vers [23]. Therefore, the high symmetry of pseudo-cubic phase is responsible for the deteriorative ferroelectricity in the ceramics $x=0.05$. Figure 6b shows P_r and E_C values of the KNNS–BZ–BNZ ceramics as a function of x. As the x increased, P_r first increased and then

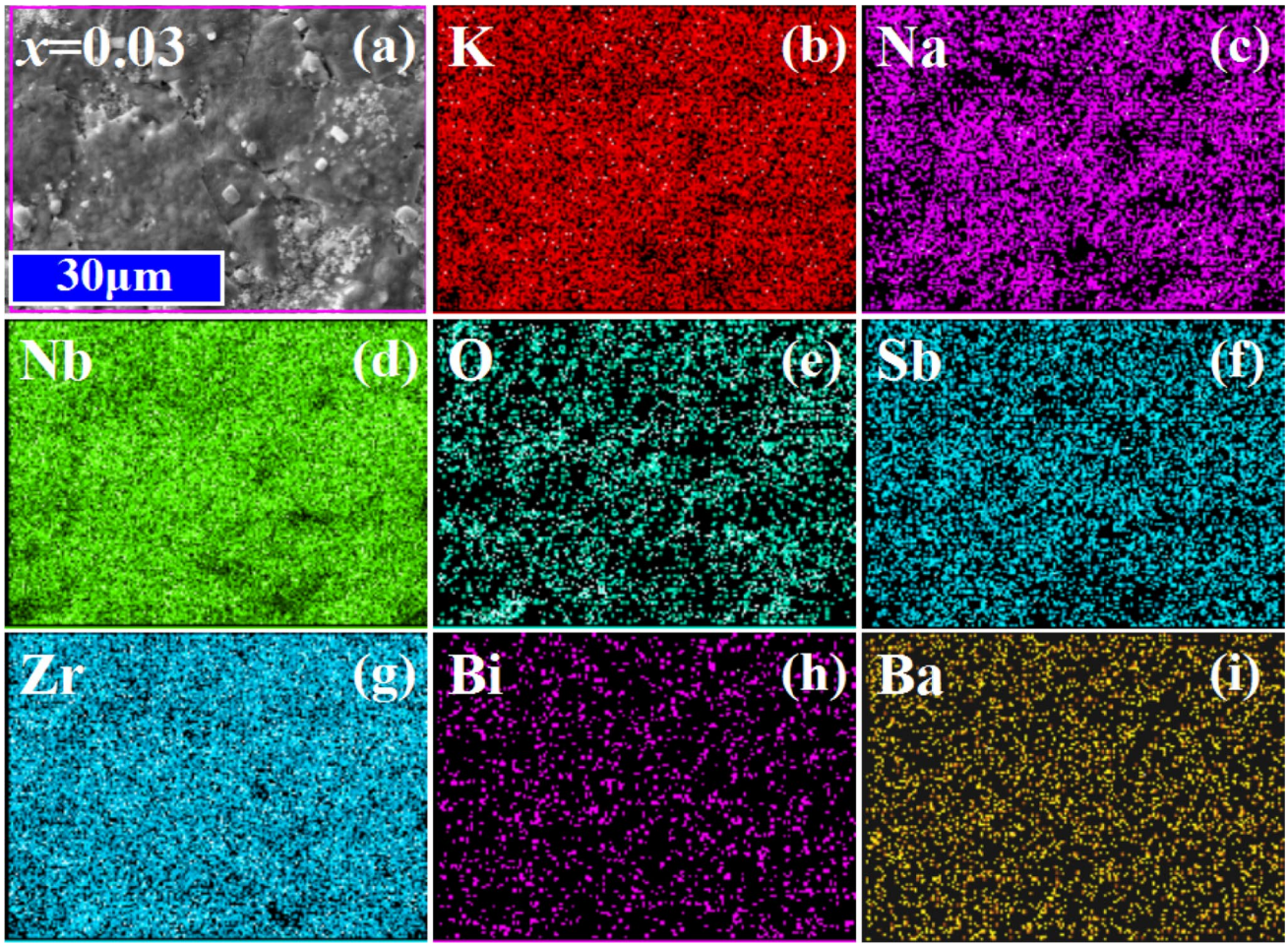

Fig. 5 **a** An selected area and **b–i** its corresponding elements (K, Na, Nb, O, Sb, Zr, Bi, Ba) mappings of the KNNS–BZ–BNZ ceramics with $x = 0.03$

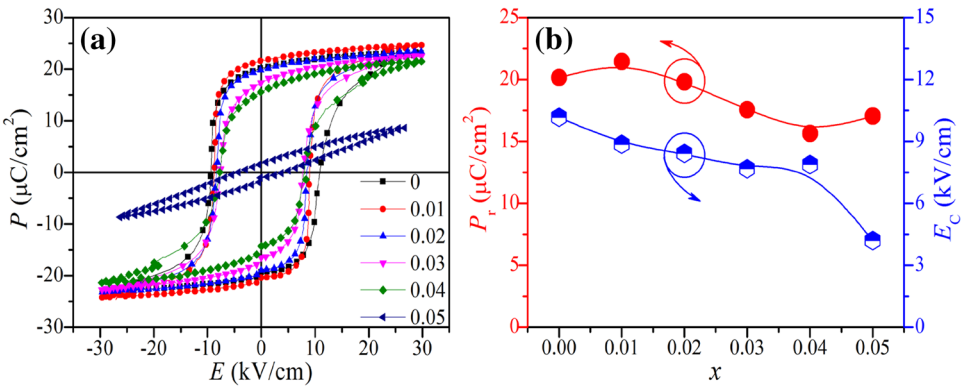

Fig. 6 **a** Ferroelectric loops and **b** P_r and E_C values of the KNNS–BZ–BNZ ceramics as a function of x

decreased, while E_C sostenuto decreased, which was consist with the previous study [24].

Figure 7 shows the dielectric constant (ε_r) and dielectric loss (tanδ) of the KNNS–BZ–BNZ ceramics varying with x values. For all ceramics, ε_r decreased and tan δ increased as the frequency increased, indicating a typical ferroelectricity [23]. For all frequencies, ε_r first increased and then decreased as the x increased, reaching the optimal value in the ceramics with $x = 0.03$ possessing an R–T coexistence phase. As for tanδ, a sostenuto increasing tendency was observed in all frequencies.

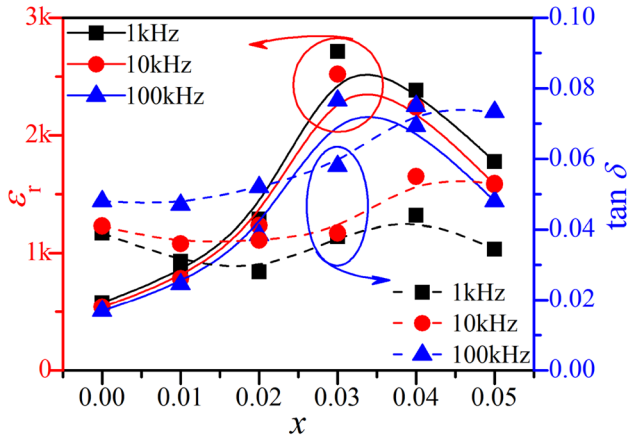

Fig. 7 Dielectric constant and dielectric loss of the KNNS–BZ–BNZ ceramics varying with x values, measured at 1, 10, 100 kHz and room temperature

In order to investigate the effect of $Bi_{0.5}Na_{0.5}ZrO_3$ on the piezoelectric properties of KNN ceramics, both d_{33} and k_p were measured, as shown in Fig. 8a. It is found that both d_{33} and k_p first increased and then dropped as the x increased, with the optimal value of 450 ± 5 pC/N and 0.50 ± 0.02 reached at $x = 0.03$ possessing an R–T phase boundary. According to previous work, both polarization rotation and domain wall motion are facilitated in the vicinity of R–T phase boundary during poling [25, 26, 34], which leads to the improved piezoelectric properties. Therefore, the enhanced piezoelectric property in this work is mainly attributed to the R–T phase boundary. In addition, the piezoelectric properties of a ferroelectric material can be evaluated by the following equation, $d_{33} \sim \alpha \varepsilon_r P_r$ [23, 27, 28]. Where α is the electrostrictive coefficient. Figure 8b plots d_{33} and $\varepsilon_r P_r$ of the KNNS–BZ–BNZ ceramics as a function of x. It is found that both d_{33} and $\varepsilon_r P_r$ should display a similar change tendency, which is well consistent with the equation. Therefore, except for the R–T phase boundary, the enhancement of ε_r and P_r plays a part role in the improved piezoelectric properties [23, 27, 28].

For practical applications, the thermal stability is an important factor. Figure 9a, b show d_{33} and normalized d_{33} values of the KNNS–BZ–BNZ ceramics against the annealing temperature (T_a). It was found that d_{33} and normalized d_{33} values of all ceramics first decreased slightly before T_a reached to T_C, and then dropped sharply when T_a exceeded T_C. Despite the decreasing d_{33} values, a relatively high d_{33} of 362 pC/N was still observed when T_a reached to 180 °C in the ceramic with $x = 0.03$, indicating a well thermal stability.

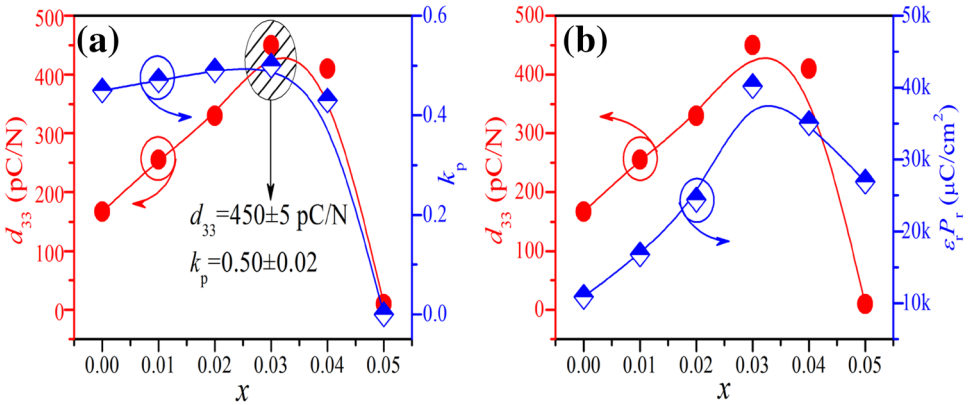

Fig. 8 **a** Piezoelectric properties (d_{33} and k_p) and **b** d_{33} *vs* $\varepsilon_r P_r$ of the KNNS–BZ–BNZ ceramics as a function of x

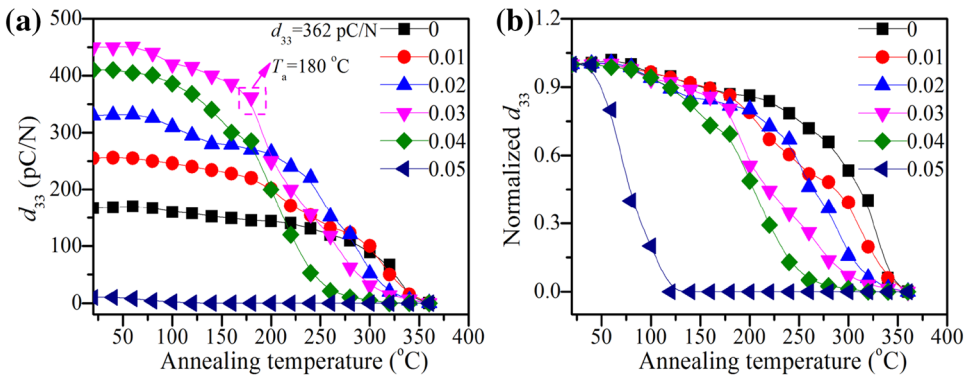

Fig. 9 **a** d_{33} and **b** normalized d_{33} values of the KNNS–BZ–BNZ ceramics against the annealing temperature

4 Conclusions

In the present work, the KNNS–BZ–BNZ lead-free piezoelectric ceramics were prepared by the conventional solid-state reaction method. The effects of $Bi_{0.5}Na_{0.5}ZrO_3$ on the phase structure, microstructure and electrical properties were systematically investigated. The results show that the addition of $Bi_{0.5}Na_{0.5}ZrO_3$ can elevate T_{R-O} and drop T_{O-T}, leading to the formation of R–T phase boundary in the ceramics with $x = 0.03$ and 0.04. The ceramics with $x = 0.03$ show the optimal piezoelectric properties, that is, $d_{33} = 450 \pm 5$ pC/N, $k_p = 0.50 \pm 0.02$. Both R–T phase boundary and the enhancement of dielectric and ferroelectric properties are attributed to the improvement of piezoelectric properties in this work. In addition, a well thermal stability is observed in the ceramics with $x = 0.03$, with a high d_{33} value of 362 pC/N as T_a reached to 180 °C. Therefore, we believe that the material system is promising for applications.

Acknowledgements Authors gratefully acknowledge the National Science Foundations of China (NSFC Nos. 51702028 and 51702029), and the supports of the Scientific Research Foundation of CUIT (Grant No. 376815).

References

1. B. Jaffe, W.R. Cook, H. Jaffe, *Piezoelectric Ceramics* (Academic, New York, 1971)
2. J. Rödel, K.G. Webber, R. Dittmer, W. Jo, M. Kimura, D. Damjanovic, J. Am. Ceram. Soc. **35**(6), 1659 (2015)
3. T.R. Shrout, S. Zhang, J. Electroceram. **19**, 111 (2007)
4. J. Rödel, W. Jo, K.T. Seifert, E.M. Anton, T. Granzow, D. Damjanovic, J. Am. Ceram. Soc. **92**(6), 1153 (2009)
5. J.G. Wu, D.Q. Xiao, J.G. Zhu, Chem. Rev. **115**, 2559 (2015)
6. J.G. Wu, D.Q. Xiao, J.G. Zhu, J. Mater. Sci. Mater. Electron. **26**(12), 9297 (2015)
7. J.F. Li, K. Wang, F.Y. Zhu, L.Q. Cheng, F.Z. Yao, J. Am. Ceram. Soc. **96**(12), 3677 (2013)
8. M. Feizpour, H.B. Bafrooei, R. Hayati, T. Ebadzadeh, Ceram. Int. **40**(1), 871 (2014)
9. B. Wu, J.G. Wu, D.Q. Xiao, J.G. Zhu, Dalton Trans. **44**(48), 21141 (2015)
10. Y. Saito, H. Takao, T. Tani, T. Nonoyama, K. Takatori, T. Homma, T. Nagaya, M. Nakamura, Nature **432**(7013), 84 (2004)
11. D. Lv, R. Zuo, J. Alloys Compd. **560**, 62 (2013)
12. F.Z. Yao, K. Wang, W. Jo, J.F. Li, Adv. Funct. Mater. **26**, 1217 (2016)
13. M.H. Zhang, K. Wang, Y.J. Du, G. Dai, W. Sun, G. Li, D. Hu, H.C. Thong, C.L. Zhao, X.Q. Xi, Z.X. Yue, J.F. Li, J. Am. Chem. Soc. **139**(10), 3889 (2017)
14. X.P. Wang, J.G. Wu, D.Q. Xiao, J.G. Zhu, X.J. Cheng, T. Zheng, B.Y. Zhang, X.J. Lou, X.J. Wang, J. Am. Chem. Soc. **136**, 2905 (2014)
15. K. Xu, J. Li, X. Lv, J.G. Wu, X.X. Zhang, D.Q. Xiao, J.G. Zhu, Adv. Mater. **28**(38), 8519 (2016)
16. R. Zuo, J. Fu, D. Lv, Y. Liu, J. Am. Ceram. Soc. **93**(9), 2783 (2010)
17. J. Wu, H. Tao, Y. Yuan, X. Lv, X. Wang, X. Lou, RSC Adv. **5**(19), 14575 (2015)
18. J. Gao, S. Ren, L. Zhang, Y. Hao, M. Fang, M. Zhang, Y. Dai, X. Hu, D. Wang, L. Zhong, J. Appl. Phys. **107**(3), 032902 (2015)
19. Z. Wang, D. Xiao, J. Wu, M. Xiao, F. Li, J. Zhu, J. Am. Ceram. Soc. **97**(3), 688 (2014)
20. Y. Wang, Q. Zhang, J. Alloys Compd. **611**, 351 (2014)
21. H. Tao, J. Wu, T. Zheng, X. Wang, X. Lou, J. Appl. Phys. **118**(4), 044102 (2015)
22. T. Zheng, J. Wu, X. Cheng, X. Wang, B. Zhang, D. Xiao, J. Zhu, X. Wang, X. Lou, J. Mater. Chem. C **2**(41), 8796 (2014)
23. J. Li, L. Fei, S. Zhang, J. Am. Ceram. Soc. **97**(1), 1 (2014)
24. X. Wang, J. Wu, D. Xiao, X. Cheng, T. Zheng, B. Zhang, X. Lou, J. Zhu, J. Mater. Chem. A **2**(12), 4122 (2014)
25. J. Gao, L. Zhang, D. Xue, T. Kimoto, M. Song, L. Zhong, X. Ren, J. Appl. Phys. **115**(5), 054108 (2014)
26. W. Liu, X. Ren, Phys. Rev. Lett. **103**(25), 257602 (2009)
27. F. Rubio-Marcos, R. López-Juárez, R.E. Rojas-Hernandez, A. Del Campo, N. Razo-Pérez, J.F. Fernandez, Acs Appl. Mater. Inter. **7**(41), 23080 (2015)
28. C. Zhao, Y. Feng, H. Wu, J. Wu, J. Alloys Compd. **666**, 372 (2016)
29. B. Wu, H.J. Wu, J.G. Wu, D.Q. Xiao, J.G. Zhu, S.J. Pennycook, J. Am. Chem. Soc. **138**, 15459 (2016)
30. J. Wu, Z. Fan, D. Xiao, J. Zhu, J. Wang, Prog. Mater Sci. **84**, 335 (2016)
31. B. Wu, J. Ma, W. Wu, M. Chen, Y.C. Ding, H.B. Tian, J. Alloys Compd. **710**, 130 (2017)
32. Z. Zhao, V. Buscaglia, M. Viviani, M.T. Buscaglia, L. Mitoseriu, A. Testino, M. Nygren, P. Johnsson, Nanni, Phys. Rev. B **70**, 024107 (2004)
33. V. Buscaglia, M.T. Buscaglia, M. Viviani, L. Mitoseriu, P. Nanni, V. Trefiletti, P. Piaggio, I. Gregora, T. Ostapchuk, J. Pokorny, J. Petzelt, J. Eur. Ceram. Soc. **26**, 2889 (2006)
34. Y. Wang, L. Hu, Q. Zhang, H. Yang, Dalton Trans. **44**(30), 13688 (2015)
35. T. Zheng, H.J. Wu, Y. Yuan, X. Lv, Q. Li, T. Men, C.L. Zhao, D.Q. Xiao, J.G. Wu, K. Wang, J.F. Li, Y.L. Gu, J.G. Zhu, S.J. Pennycook, Energy Environ. Sci. **10**, 528 (2017)